

An Observational and High-Resolution Model Analysis of Gale Wind Events in the Gulf of California

ARIEL E. COHEN

NOAA/National Weather Service/Weather Forecast Office, Jackson, Mississippi

JOHN P. CANGIALOSI

NOAA/National Weather Service/National Hurricane Center, Miami, Florida

(Manuscript received 15 June 2009, in final form 15 October 2009)

ABSTRACT

The Tropical Analysis and Forecast Branch (TAFB) of the National Oceanic and Atmospheric Administration's (NOAA's) National Hurricane Center in Miami, Florida, provides high-seas forecasts to portions of the eastern Pacific Ocean, including the Gulf of California. These forecasts include wind velocity and significant wave height forecasts and are initiated by forecast winds of at least 20 kt (10.3 m s^{-1}) or significant wave heights of at least 8 ft (2.4 m). The Gulf of California is a commonly traveled area, where winds are highly modulated by nearby terrain variations. This provides a unique forecast challenge, especially in the absence of regular surface observations. In October and November 2008, the NOAA R/V *David Starr Jordan* was stationed in the Gulf of California and occasionally reported gale force winds [$34\text{--}47 \text{ kt}$ ($17.5\text{--}24.2 \text{ m s}^{-1}$)], which operational models regularly missed. A ship log of these events provided the basis for determining mean and anomaly fields for a handful of meteorological variables, from which a conceptual model for the synoptic-scale environment supporting these events is presented. An index based on the mean sea level pressure (MSLP) difference between Ely, Nevada, and Yuma, Arizona, was developed to measure the potential for gales, which was found to be statistically significant in discriminating between "gale" and "marginal wind" events. The fifth-generation NCAR–Pennsylvania State University Mesoscale Model (MM5) is used to conduct doubly nested high-resolution simulations centered on the Gulf of California. These simulations appeared to resolve the gales better than traditional global model guidance, lending credence toward the need for high-resolution modeling in areas of highly variable terrain. Relatively small errors were found in MM5 output using the National Aeronautics and Space Administration (NASA) Quick Scatterometer (QuikSCAT) data as verification.

1. Introduction

Forecasters at the Tropical Analysis and Forecast Branch (TAFB) of the National Oceanic and Atmospheric Administration's (NOAA) National Hurricane Center in Miami, Florida, are responsible for providing high-seas forecasts to the Gulf of California, also known as the Sea of Cortez. High-seas forecasts provide event-driven forecasts of strong wind [20 kt (10.3 m s^{-1}) or higher] and high-wave [8 ft (2.4 m) or higher] areas. The gulf is an oft-traversed waterway and provides a particularly unique challenge to forecasters due to local wind

enhancements driven by the highly variable terrain that bounds the gulf.

As is the case across much of intermountain western United States, the scarcity of in situ observations across the gulf provides forecasters with little chance of verifying both wind and wave forecasts. Forecasters have generally relied on global models, both operational and ensemble, to provide wind and wave forecasts for this region without having much idea as to their verification. However, scatterometer data provide useful clues for short-term forecasting and verification. Some of these scatterometer data are collected from the National Aeronautics and Space Administration (NASA) Quick Scatterometer (QuikSCAT) satellite and the European Space Agency's Advanced Scatterometer (ASCAT) satellite. In addition to the National Hurricane Center's reliance on QuikSCAT data for diagnosing the size, intensity,

Corresponding author address: Ariel Cohen, NOAA/National Weather Service/Weather Forecast Office, 234 Weather Service Dr., Flowood, MS 39232.
E-mail: ariel.cohen@noaa.gov

and locations of tropical cyclones, QuikSCAT retrievals provide critical wind data across much of TAFB's area of responsibility (Brennan et al. 2009). Not only does QuikSCAT provide valuable ocean wind vector information for forecasters at NHC, but it is also regularly used by NOAA's Ocean Prediction Center (e.g., Chelton et al. 2006; Von Ahn et al. 2006) and by the Australian Bureau of Meteorology's Regional Forecast Center (RFC) and Tropical Cyclone Warning Center (TCWC) (Leslie et al. 2008).

Forecasters also rely on their own understanding of global wind climatologies and their supporting synoptic fields to provide better forecast accuracy. These climatologies have been summarized in the Scatterometer Climatology of Ocean Winds (SCOW; Risien and Chelton 2008). SCOW uses QuikSCAT surface winds to derive seasonal wind climatologies from September 1999 to August 2007, providing global and seasonal cycles of 12 variables, including wind stress and derivatives thereof. Local enhancements to surface wind stress in TAFB's area of responsibility are highlighted in SCOW, including those in the Gulfs of Tehuantepec and Papagayo. Interestingly, the Gulf of California challenge is somewhat similar to the Gulf of Tehuantepec challenge (Cobb et al. 2002) in that both are driven by somewhat similar synoptic regimes, though the scatterometer defects are more pronounced in the Gulf of California, where there is a greater land influence. However, as Risien and Chelton (2008) acknowledge, SCOW is limited in the sense that seasonal wind cycles only explain a small part of the total variation of the winds at many locations. Thus, the present study is intended to add greater understanding of local wind variations (i.e., over the Gulf of California) to our global wind knowledge. Unfortunately, as Brennan et al. (2009) point out, QuikSCAT data are associated with a number of sampling defects, including the low frequency of passes at any given location, as well as the large gaps between swaths in the tropics. In some cases, ship observations fill in these gaps.

In autumn 2008, forecasters were surprised a number of times when a ship meandering in the northern gulf reported northwest to north surface winds over gale force while all global model guidance was depicting 10-m winds no higher than 25 kt (12.9 m s^{-1}). Forecasters investigated these observations and found that they originated from the NOAA Research Vessel (R/V) *David Starr Jordan*, whose primary mission was to study the biological and physical oceanography of the Gulf of California in autumn 2008. This mission also provided meteorological measurements that were of particular help to forecasters at TAFB. Forecasters immediately questioned the quality of the observations, given their consistent high bias relative to the model output. However, after a number

of events and realizing the credibility of the observations from the *David Starr Jordan*'s calibrated wind sensor, analysis revealed that particular synoptic patterns over the midlatitudes consistently occurred with these reported gale wind events. Additionally, anecdotal evidence of these wind events are provided in Williams (1996), which suggests frequent gale force wind events in the Gulf of California during autumn time. Given this additional evidence, TAFB forecasters quickly realized that global models insufficiently resolved these gap wind events, as well as many other gap wind events across the Intermountain West (e.g., Mass and Albright 1985; Sharp and Mass 2002). This led to recent initiatives to investigate the synoptic-scale and mesoscale environments that support the gale wind events as recorded by the R/V *David Starr Jordan*, the results of which are presented in the following sections. We present forecast tools based on observations and high-resolution modeling.

2. Methodology

Given the absence of frequent wind observations and inadequate model forecasts of low-level winds in the Gulf of California, TAFB forecasters have come to rely on a conceptual model developed in this study to provide techniques in synoptic-scale pattern recognition that global models can more adequately resolve. Synoptic pattern recognition is invaluable in forecasting these events and can be applied to any global models, which are known to insufficiently resolve the low-level momentum fields for these events at the mesoscale level (e.g., Sharp and Mass 2002).

To identify meteorological patterns associated with gale wind events, as well as nongale wind events, we developed a set of criteria to stratify wind speed data provided on an hourly basis by the R/V *David Starr Jordan* after the conclusion of its mission. We chose to call a "gale event" a day during which at least three consecutive hours were logged with gale force winds [i.e., sustained winds of 34–47 kt (17.5 to 24.2 m s^{-1})], and we chose to call a "marginal wind event" a day during which at least 3 h (not necessarily consecutive) were logged with winds of 15–25 kt (7.7 – 12.9 m s^{-1}), but no gale force winds were reported. We excluded shorter-duration gales because forecast periods in the high-seas forecast product span at least 3 h in most cases. There are certainly many other stratification schemes we could have used. However, our goal is to distinguish the more high-impact gale events from the minimal threshold for inclusion in the high-seas forecast product [i.e., winds of 20 kt (10.3 m s^{-1}); National Weather Service (2008)].

Based on our criteria, we found a total of seven gale events (Gs) and seven marginal wind events (MWs).

TABLE 1. Summary of gale events recorded by the NOAA R/V *David Starr Jordan*, except the 10 Jan 2009 event based on QuikSCAT data.

Date	Time of max wind (UTC)	Max wind (kt)
13 Oct 2008	1000	37
14 Oct 2008	1100	38
22 Oct 2008	1100	40
6 Nov 2008	2400	42
15 Nov 2008	0900	45
10 Jan 2009	1200	37

TABLE 2. Summary of marginal wind events recorded by the NOAA R/V *David Starr Jordan*.

Date	Time of max wind (UTC)	Max wind (kt)
5 Oct 2008	0100	21
10 Oct 2008	1200	24
20 Oct 2008	1000	17
12 Nov 2008	1100	20
18 Nov 2008	1100	15
21 Nov 2008	1200	18
26 Nov 2008	1200	17

Tables 1 and 2 summarize these events. We used the National Centers for Environmental Prediction–National Center for Atmospheric Research (NCEP–NCAR) global reanalysis (Kalnay et al. 1996) composite data provided by the NOAA/Earth System Research Laboratory’s (ESRL) Physical Sciences Division (PSD) to create mean and anomaly plots of several meteorological variables for Gs and MWs. The most distinguishing features between the Gs and MWs are found in the 500-hPa height, mean sea level pressure (MSLP), lifted index (LI), and 850-hPa temperature fields (Figs. 1 and 2). Upon postanalysis, we excluded one G that appeared to be supported by an atypical synoptic pattern, which is discussed later. Composite mean fields are computed by calculating the mean of each variable among all recorded G or MW dates. Anomaly fields are computed by calculating the departure of each variable from its climatological average between 1968 and 1996 on a case-by-case basis followed by averaging the anomalies.

3. Conceptual model

Figure 1 provides mean and anomaly 500-hPa heights for G and MW cases. For the Gs, anomalously strong 500-hPa ridging appears to be associated with a highly amplified, long-wave 500-hPa ridge over the eastern Pacific and west coast of the United States, with a medium-wavelength 500-hPa trough over the central United States. We can infer that strong differential negative vorticity advection downstream of the 500-hPa ridge axis supports deep-layer subsidence over the Rocky Mountains, which results in the development of anomalously strong surface high pressure as seen in the MSLP fields for G cases in Fig. 2. These 500-hPa and surface patterns are also associated with the positive phase of the Pacific–North American pattern, which is also known to support gale wind events in the Gulf of Tehuantepec (Cobb et al. 2002). For the MW cases, 500-hPa waves show less amplitude, with no particularly strong anomalies in either the MSLP or 500-hPa fields.

The strong surface high depicted for Gs in Fig. 2, centered over the northern Rockies, is north of a 850-hPa front as seen in Fig. 3. The 850-hPa level was chosen to diagnose near-surface frontal passage, as it provides an approximate pressure for the surface in the west-central and southwest continental United States (CONUS). The 850-hPa front surges south or southwestward into the northern Gulf of California at the leading edge of the airmass anchored by the strong surface high over the northern Rockies. The presence of a low-level baroclinic zone is even more apparent in the LI field for Gs, as seen in Fig. 4. Low-level cold-air advection behind the 850-hPa front is capped by warmer air aloft under subsiding 500-hPa flow downstream of the 500-hPa ridge axis over the eastern Pacific. That juxtaposition yields anomalously positive LIs for the Gs.

In addition, the low-level cold-air advection, which is capped by an inversion that drives the strong positive LIs for the G cases, likely generates steep low-level lapse rates over the relatively warmer northern Gulf of California waters during the autumn. These steeper lapse rates generate turbulent kinetic energy and stronger winds, particularly gusts, beneath a stable layer that also traps wave energy. Figure 5 presents the 0000 UTC sounding from Tucson, Arizona, on 15 November 2008, when a G was ongoing. The thermal sounding shows a frontal inversion around 800 hPa, generating deep-layer stability and a lifted index around 12.5°C. This sounding, which depicts a near-surface superadiabatic lapse rate at Tucson, can be somewhat representative of the sounding at that time over the northern Gulf of California. While the superadiabatic layer in this sounding is the result of strong diurnal heating at Tucson, a similar superadiabatic layer could be driven by the above-surface air being advected over the warmer waters in the northern Gulf of California. In the absence of frictional dampening, the superadiabatic layer over the Gulf of California could be more efficient at realizing boundary layer turbulence and stronger surface winds than at Tucson, where frictional effects would dampen the turbulence. An analogous scenario occurs when stronger low-level winds are

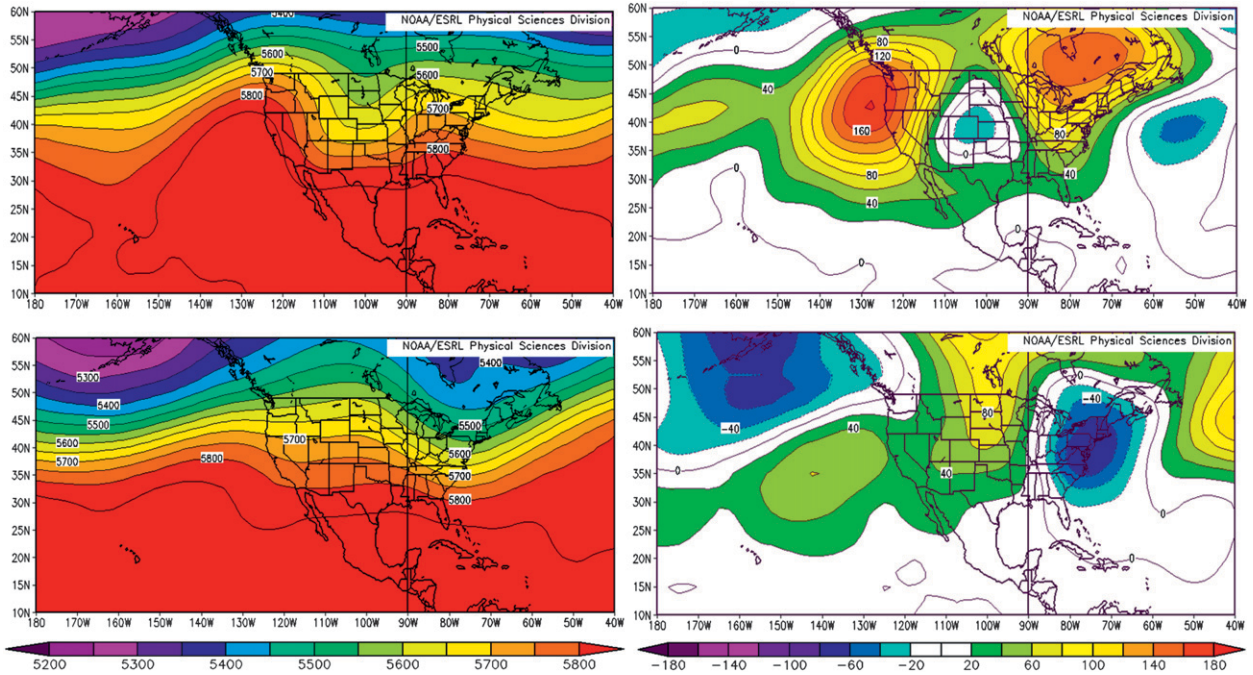


FIG. 1. Composite (left) mean and (right) anomaly 500-hPa heights (gpm) for (top) G and (bottom) MW cases.

driven by reduced low-level static stability when cooler air overlays the warmer Gulf Stream waters, resulting in increased surface wind stress (Von Ahn et al. 2006). Additionally, the relationship between low static stability, sea surface temperatures, and surface wind stress

is documented in Chelton et al. (2001) and Risien and Chelton (2008) using QuikSCAT winds, which was also previously discussed in Wallace et al. (1989). Significant efforts have been made to raise awareness among forecasters at the Ocean Prediction Center (Von Ahn et al.

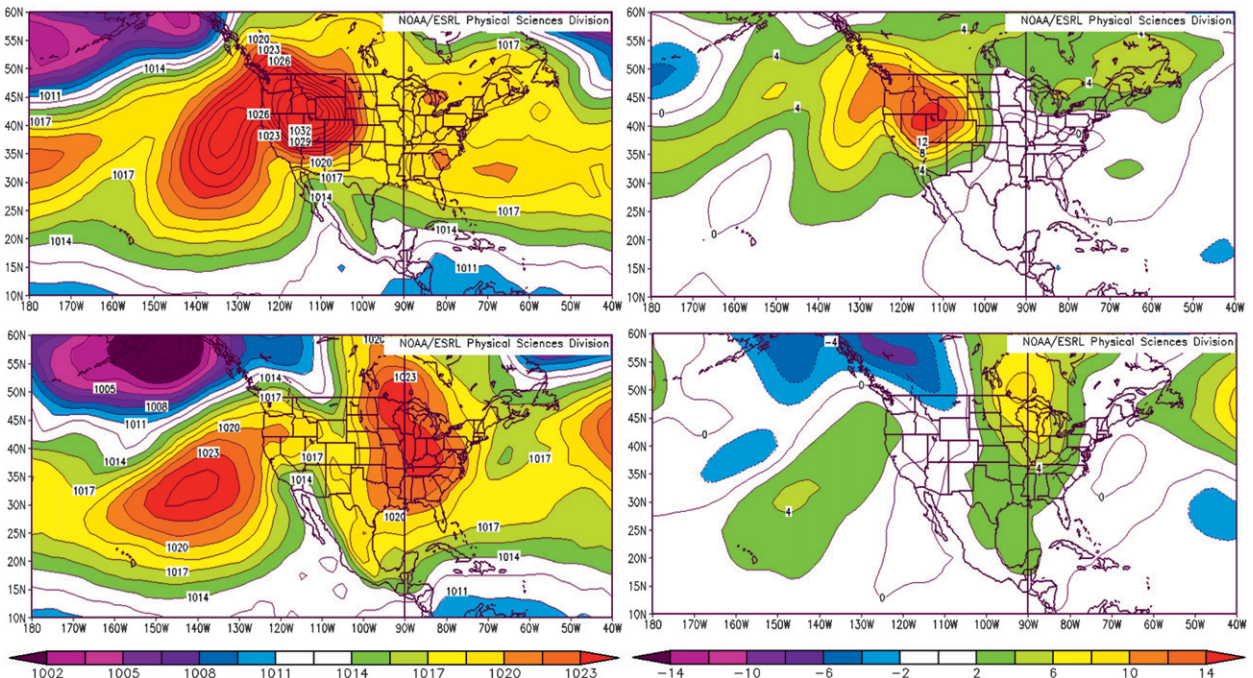


FIG. 2. Composite (left) mean and (right) anomaly MSLP (hPa) for (top) G and (bottom) MW cases.

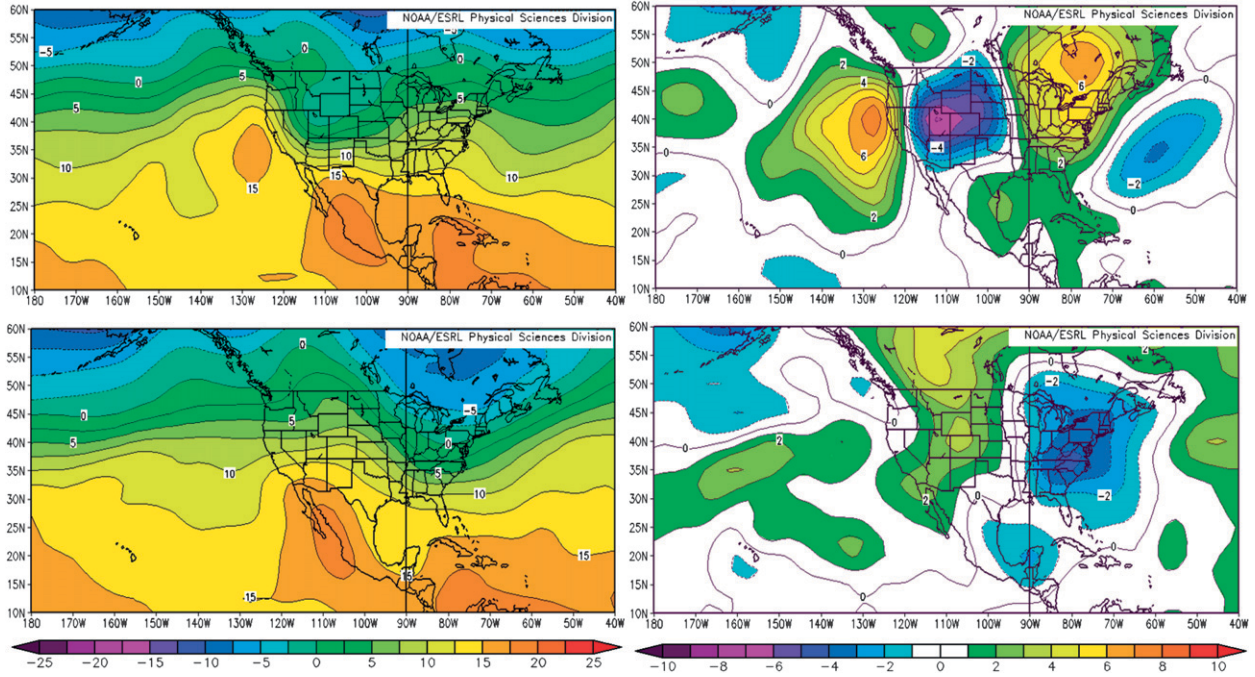


FIG. 3. Composite (left) mean and (right) anomaly 850-hPa temperatures ($^{\circ}\text{C}$) for (top) G and (bottom) MW cases.

2006) and the National Hurricane Center regarding the forecast implications of these interactions, and as well as to further explain the scatterometer data.

It is the combination of the aforementioned synoptic features and the unique topography over the western United States and Mexico that favors gale wind events in

the Gulf of California. Figure 6 provides the 0600 UTC synoptic surface chart on 10 January 2009. A 1041-hPa high pressure system was situated over the Great Basin of the United States and a stationary front was located across northwestern Mexico. These are the synoptic surface features discussed above (Fig. 2) that supported one of the

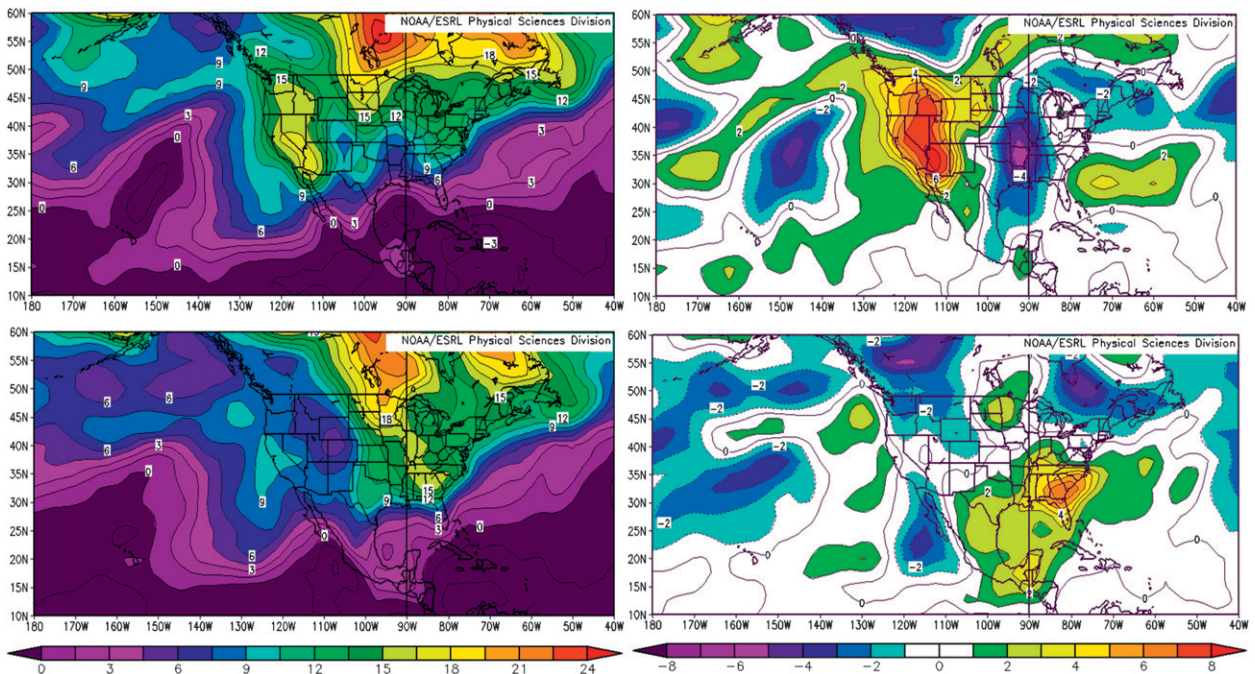


FIG. 4. Composite (left) mean and (right) anomaly surface-based LIs ($^{\circ}\text{C}$) for (top) G and (bottom) MW cases.

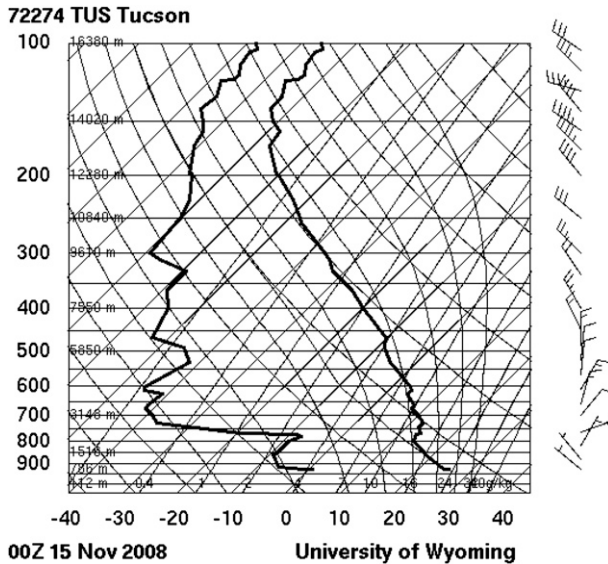


FIG. 5. Tucson, AZ, 0000 UTC sounding on 15 Nov 2008 (University of Wyoming 2008). Contours most steeply sloped from bottom left to top right are of constant temperature ($^{\circ}\text{C}$) and less steeply sloped from the same direction are of constant mixing ratio (g kg^{-1}). Contours most steeply sloped from bottom right to top left are of constant dry potential temperature and least steeply sloped from bottom right to top left are of constant equivalent potential temperature. Horizontal lines denote pressure and height, with the rightmost boldface curve indicating environmental temperature and the leftmost boldface curve indicating the environmental dewpoint temperature ($^{\circ}\text{C}$) profile.

gales studied in the northern Gulf of California. Figure 7 presents the geographical layout that supports the Gs. The Gulf of California lies in the north-northwest–south-southeast valley bounded by the Sierra Madre Occidentals to the east, the higher terrain of the Intermountain West to the north, and the Baja California Mountains to the west. The meridional component of motion is driven by the strong north–south pressure gradient force between the strong surface high pressure over the northern Rockies and lower pressure over the gulf. This flow is then further accelerated by the perturbation pressure gradient force driven by the orientation of the gulf relative to the aforementioned pressure gradient considering mass conservation principles. Furthermore, downslope flow off higher terrain to the north accelerates the flow. Finally, maximum winds were found between 1000 and 1200 UTC [0200 and 0400 Pacific standard time (PST)], when katabatic drainage flow off surrounding higher terrain is maximized by the presence of clear skies (as inferred, e.g., from total precipitable water products and infrared satellite).

4. Gulf of California gale wind potential index

Based on the pattern that links the strong surface pressure gradient over the southwest United States to

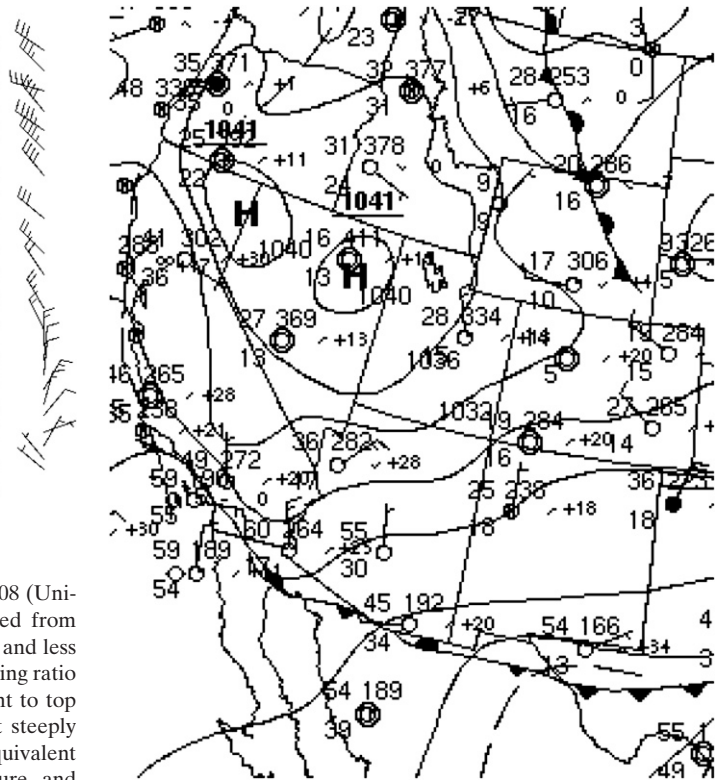


FIG. 6. The 0600 UTC synoptic surface chart from 10 Jan 2009, isobars contour interval (CI) 4 mb.

gale wind events, we attempted to find combinations of western U.S. MSLP observations that capture this gradient and that best discriminate between the Gs and the MWs. Of all of the combinations, the difference in MSLP between Ely, Nevada, and Yuma, Arizona, best discriminates between the Gs and the MWs, with a P value of 0.001 and a 50th percentile of around 12–13 hPa for Gs. We will call this the Gulf of California gale wind potential index. The small sample size required us to use a two-sample *t* test, which assumes unequal variances to derive a P value. We agree that this sample is not as statistically robust as we would like, and a larger dataset would likely lend more credence to this study's results. Nevertheless, we feel this index is physically grounded and sufficiently discriminates between the Gs and the MWs for short-term forecasting. Among our six G cases and seven MW cases, the differences in MSLP between Ely and Yuma (taken as Ely–Yuma) are summarized in the box-and-whiskers plot in Fig. 8, which provides 0th, 25th, 50th, 75th, and 100th percentiles for the G and MW cases (0th and 25th percentiles are identical for the MW cases). Figure 8 shows the large spread in this index between the G events and the MW events, and indicates some reliability in the discriminatory power of this index between these two classes of events.



FIG. 7. Relief map illustrating the geographical layout that supports the Gs. Elevated surfaces indicate higher terrain (National Geophysical Data Center 2009).

To compare the Gulf of California gale wind potential index against ship-observed wind speeds from the R/V *David Starr Jordan*, we plot 1200 UTC wind speed and gale wind potential index measurements in Fig. 9. We choose to plot only daily measurements that reflect synoptic-scale fluctuations in these parameters, as opposed to diurnal cycles that appear to add noise to the data. The time of 1200 UTC was chosen because it is around the time of peak winds (though not necessarily of gale force, as seen in Fig. 9), it constitutes a forecast period in the high-seas forecast, and many global and regional numerical weather prediction models are initialized at

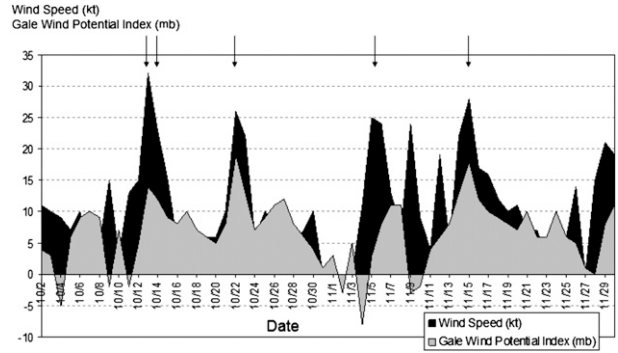


FIG. 9. Daily time series analyses of ship wind speed and gale wind potential index (Gs are specified with arrows). Horizontal axis times are at 1200 UTC for the date listed.

this time. We see that peaks in the Gulf of California gale wind potential index and the wind speeds are well correlated in time, though without much lead time. However, since global models generally accurately resolve large-scale synoptic mass fields, particularly for short-term forecasting purposes, such an index could be used in a prognostic mode. In a few cases, G-supporting indices only support MWs or neither Gs or MWs (e.g., 8 and 26 October and 17 and 21 November), and additional factors need to be considered in the forecast process for Gulf of California wind events (e.g., thermodynamic structure of the postfrontal air mass). In fact, the correlation coefficient between the index and the corresponding wind speeds is low (i.e., 0.264); however, we speculate that this

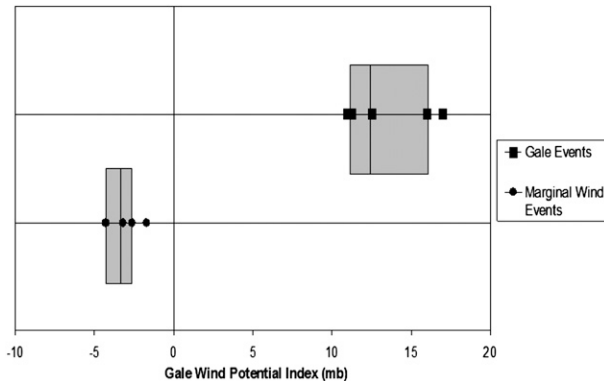


FIG. 8. Box-and-whiskers plots for G and MW cases, presenting the 0th, 25th, 50th, 75th, and 100th percentiles of each separate dataset.

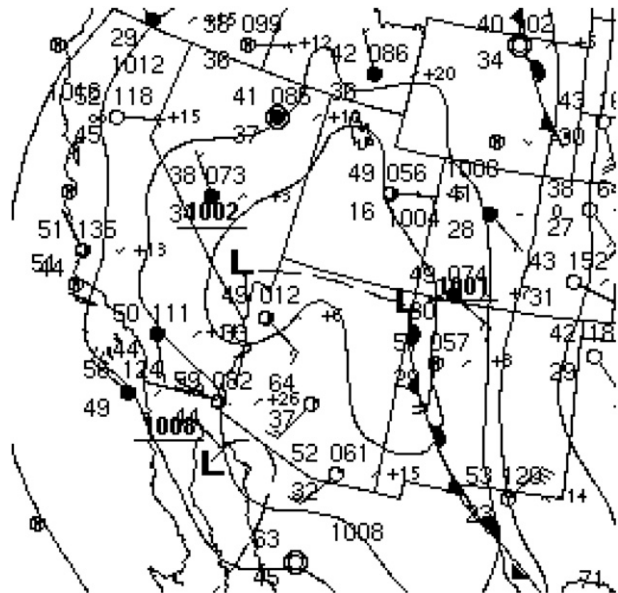


FIG. 10. The 0600 UTC synoptic surface chart 11 Apr 2009 CI 4 mb.

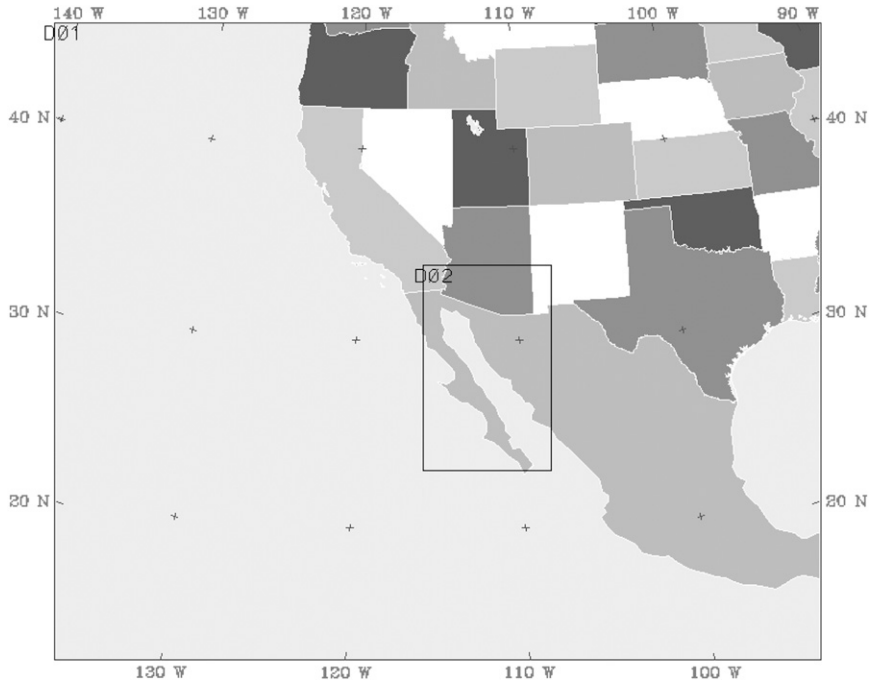


FIG. 11. Domain configuration for MM5 runs.

reflects the inability of this index to discriminate among weaker wind events. Such an index needs to be considered as merely guidance in this forecast process and could be used in conjunction with high-resolution model forecasts to more accurately forecast these events.

5. Anomalous case

Gale wind events in the Gulf of California that do not fit the pattern described above have rarely been reported. However, one exception involves a deep trough over the

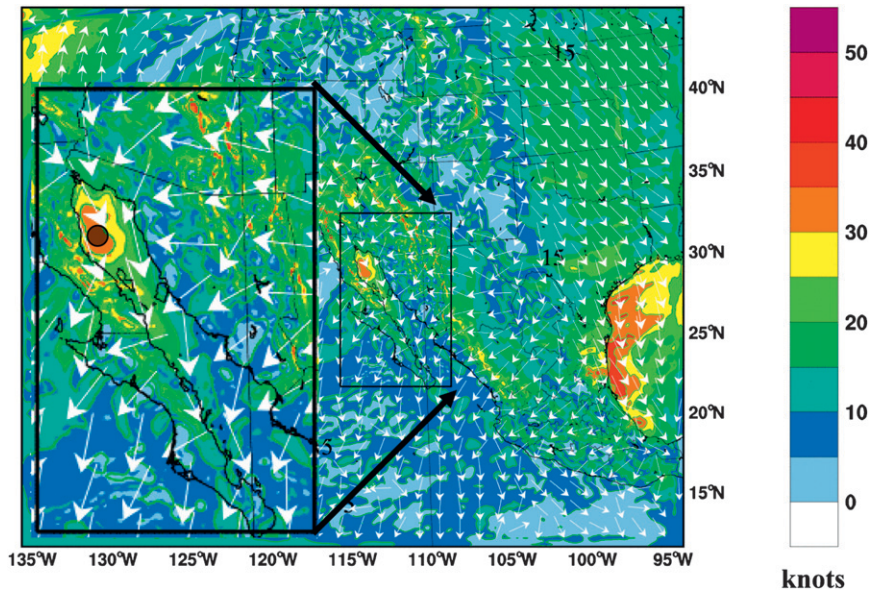


FIG. 12. MM5 10-m wind speed output for a simulation initialized at 0000 UTC 14 Nov 2008 and valid at 1200 UTC 15 Nov 2008 (a 36-h forecast), with the dot indicating the approximate position of the R/V David Starr Jordan at this time.

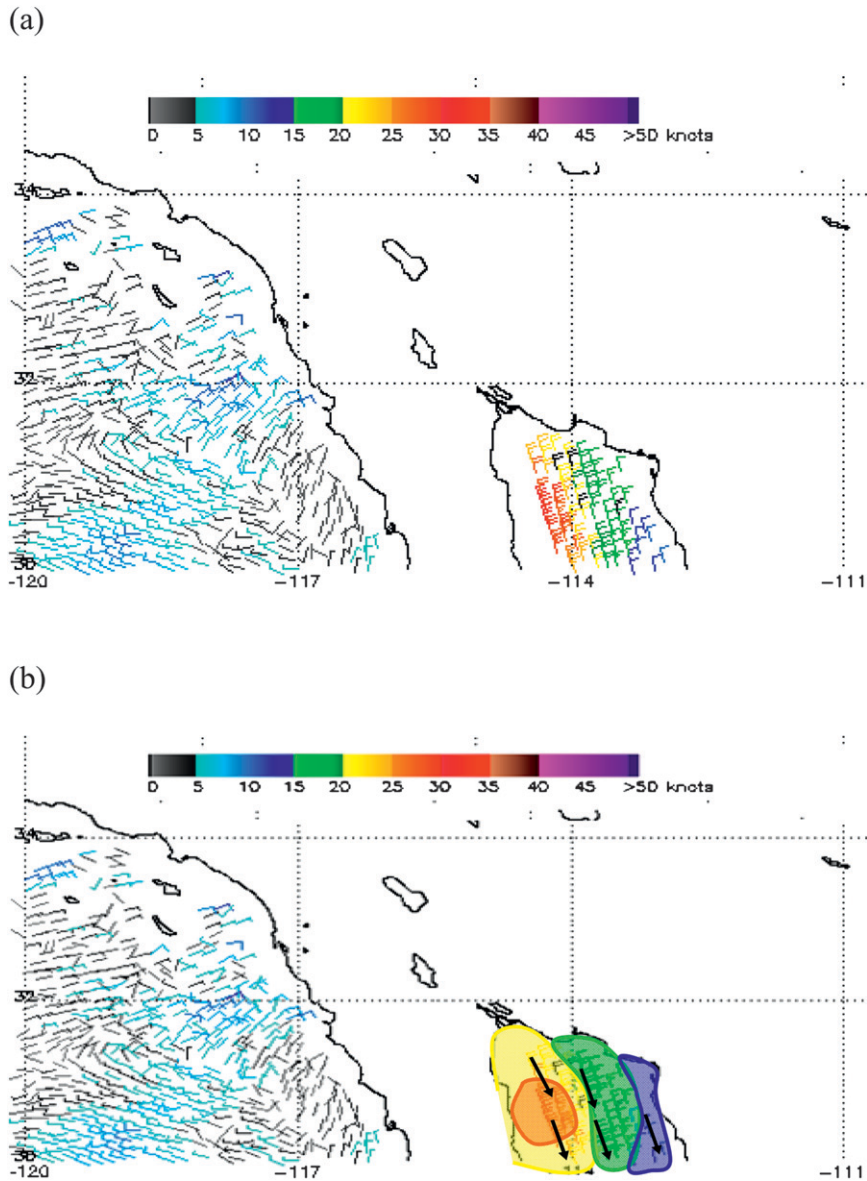


FIG. 13. (a) Corresponding QuikSCAT data around 1330 UTC 15 Nov 2008, which provide swaths of ocean wind vectors from the polar-orbiting QuikSCAT satellite. (b) As in (a), but with approximate isotachs (blue indicating 10–14 kt, green indicating 15–19 kt, yellow indicating 20–29 kt, and orange indicating 30+ kt) and arrows plotted in the Gulf of California for comparison with Figs. 12 and 14.

western United States with a strong low- to midlevel jet streak in the base of the trough that is forced to down-slope off the Baja California Mountains into the Gulf of California. This case could also be associated with deepening low pressure over the southwest United States or over the northern Gulf of California, as depicted in Fig. 10. Surface winds in these situations are found to occasionally reach gale force based on scatterometer data, with the primary wind direction being southwesterly. We speculate that this southwesterly flow is accelerated by

terrain-driven downslope processes, with the southerly component being accelerated by funneling along the long axis of the Gulf of California.

6. High-resolution modeling

In the preceding sections, we have developed a general conceptual model that forecasters can use to understand synoptic conditions favorable for higher-impact gale wind events in the Gulf of California. The development of this

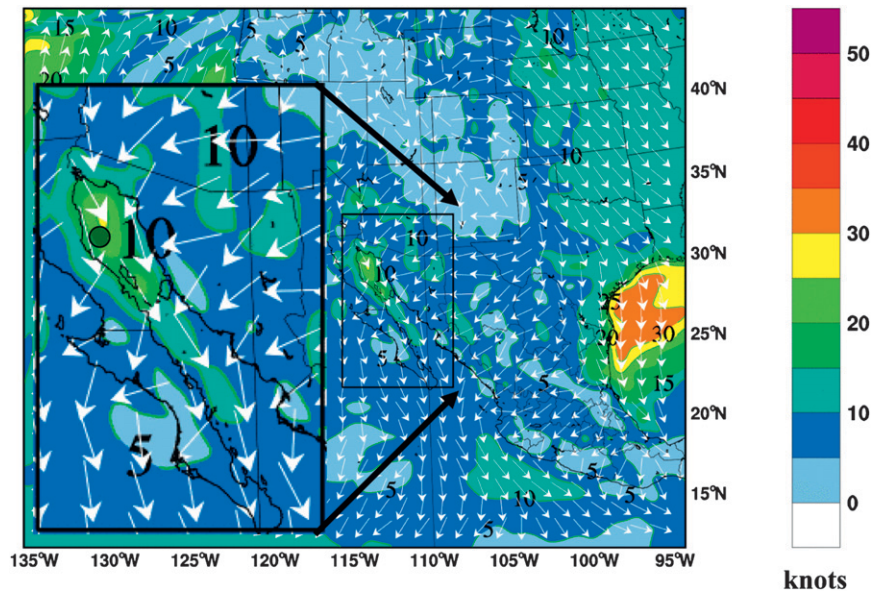


FIG. 14. GFS 10-m wind speed output for a simulation initialized at 0000 UTC 14 Nov 2008 and valid at 1200 UTC 15 Nov 2008 (a 36-h forecast), with the dot indicating the approximate position of the R/V *David Starr Jordan* at this time.

conceptual model provides a method for pattern recognition using global models. However, these global models are known to inadequately resolve the magnitude and spatial distribution of these events due to their relatively coarse resolution and resultant inability to resolve fine-scale topographical variations. Despite these limitations, TAFB forecasters have used meteorological model output at multiple levels in the atmosphere (e.g., 30-, 60-, and 925-mb levels) to forecast the potential for higher-momentum air aloft to be transported to the surface for gap wind events [e.g., Gulf of Tehuantepec; Cobb et al. (2002)]. In this section, we will explore the usefulness of a high-resolution model [i.e., the fifth-generation NCAR–Pennsylvania State University Mesoscale Model (MM5)] to simulate gap wind events in the Gulf of California.

We use the high-resolution, nonhydrostatic MM5 to simulate winds in the Gulf of California for a few cases revealed by the R/V *David Starr Jordan*. This version of the MM5 (Grell et al. 1994) has been used to simulate a number of related gap wind events (e.g., Schultz et al. 1997). We chose a model configuration that used two nested domains. The outer domain used a horizontal grid resolution of 15 km (300 grid points \times 300 grid points), while the inner domain used a horizontal grid resolution of 5 km (211 grid points \times 103 grid points) and encompasses the Gulf of California (Fig. 11). Both domains were forced to interact with each other in a two-way feedback process. Both domains used 30 vertical sigma levels, with 11 sigma levels in the planetary boundary layer. The Global Forecast System (GFS) forecast fields

(Kalnay et al. 1990), including Reynolds' weekly sea surface temperatures (SSTs), provided the initial and lateral boundary conditions for the domains (Reynolds and Smith 1994).

The first simulation we will consider was for an event that occurred on 15–16 November 2008. We present the results of the 96-h-long simulation that was initialized at 0000 UTC 14 November 2008, about 36–48 h prior to the peak of the wind event based on ship observations (i.e., the approximate maximum warning lead time that is currently provided by the high-seas forecast). Figure 12 provides 10-m wind speed output from the MM5 for 1200 UTC 15 November 2008, while Fig. 13 provides verification from a QuikSCAT pass around 1330 UTC 15 November 2008. Note that the R/V *David Starr Jordan* recorded winds at 22.9 m above sea level. It is immediately apparent that the MM5 provided a remarkably realistic and reliable depiction of the strength and geographical distribution of this wind event. Maximum winds forecast by the MM5 and verified by the QuikSCAT pass were 35 kt (18.0 m s^{-1}). The 10-m wind velocity output from the GFS is provided in Fig. 14 for comparison, which inadequately forecasts the intensity during this event.

With wind speed data provided by the R/V *David Starr Jordan*, we can compare forecast wind speeds derived from the MM5 and GFS with those measured by data collected by the R/V *David Starr Jordan*. Figure 15 shows a meteogram that compares observed wind speeds from the ship and 10-m wind speeds forecast by the MM5 and GFS for the 0000 UTC 14 November 2008

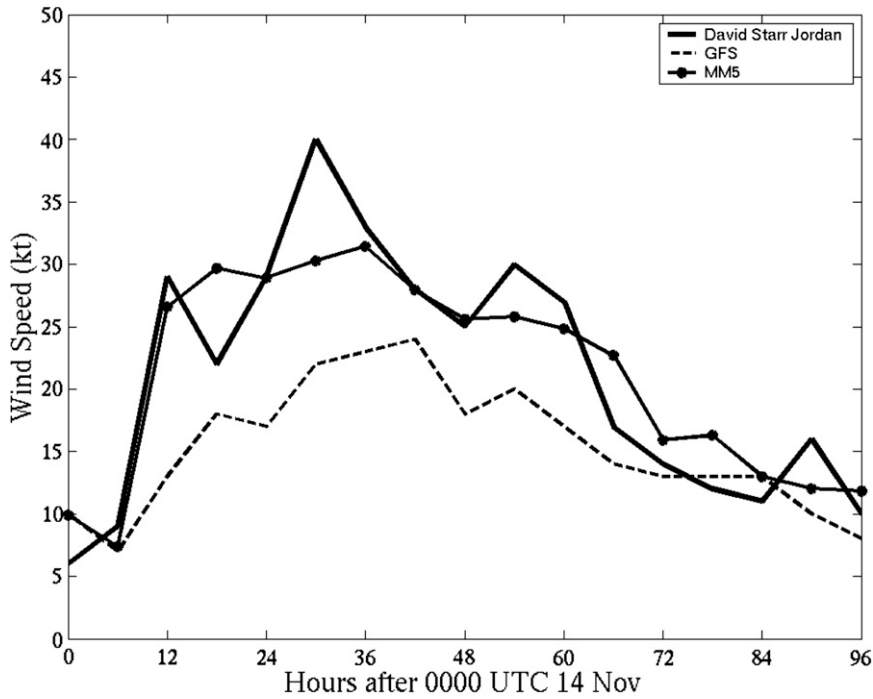


FIG. 15. Meteogram comparing 10-m wind speeds derived from the MM5 and GFS for points along the path of the ship, with the corresponding wind speeds measured from the ship.

initialization. We extracted the forecast wind speeds based on MM5 and GFS output at the closest grid point to the ship as it traversed the Gulf of California. These forecast wind speeds are then compared to the wind

speeds as measured by the ship, providing us with a ship-following verification dataset.

The agreement between MM5 output and ship observations is remarkably good for the duration of the

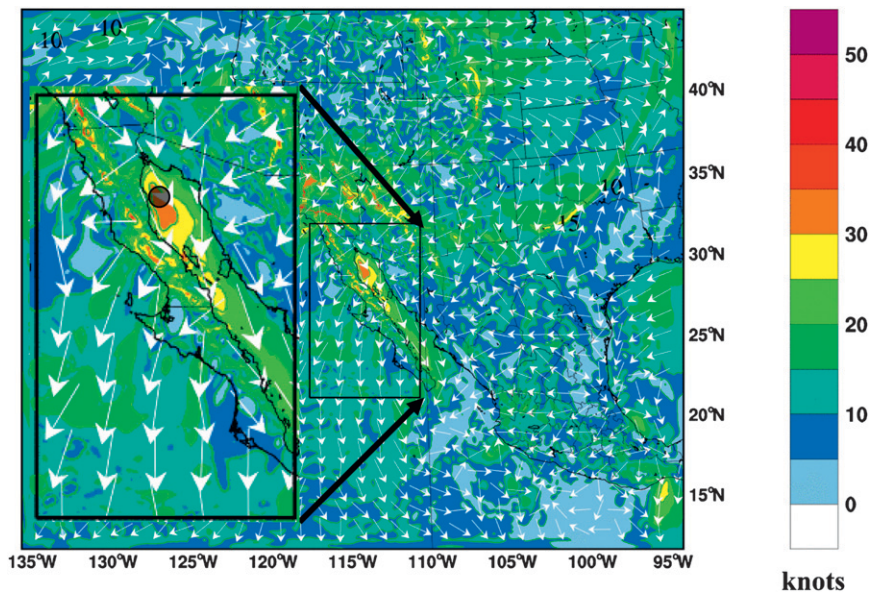


FIG. 16. MM5 10-m wind speed output for a simulation initialized at 0000 UTC 11 Oct 2008 and valid at 1200 UTC 14 Oct 2008 (an 84-h forecast), with the dot indicating the approximate position of the R/V *David Starr Jordan* at this time.

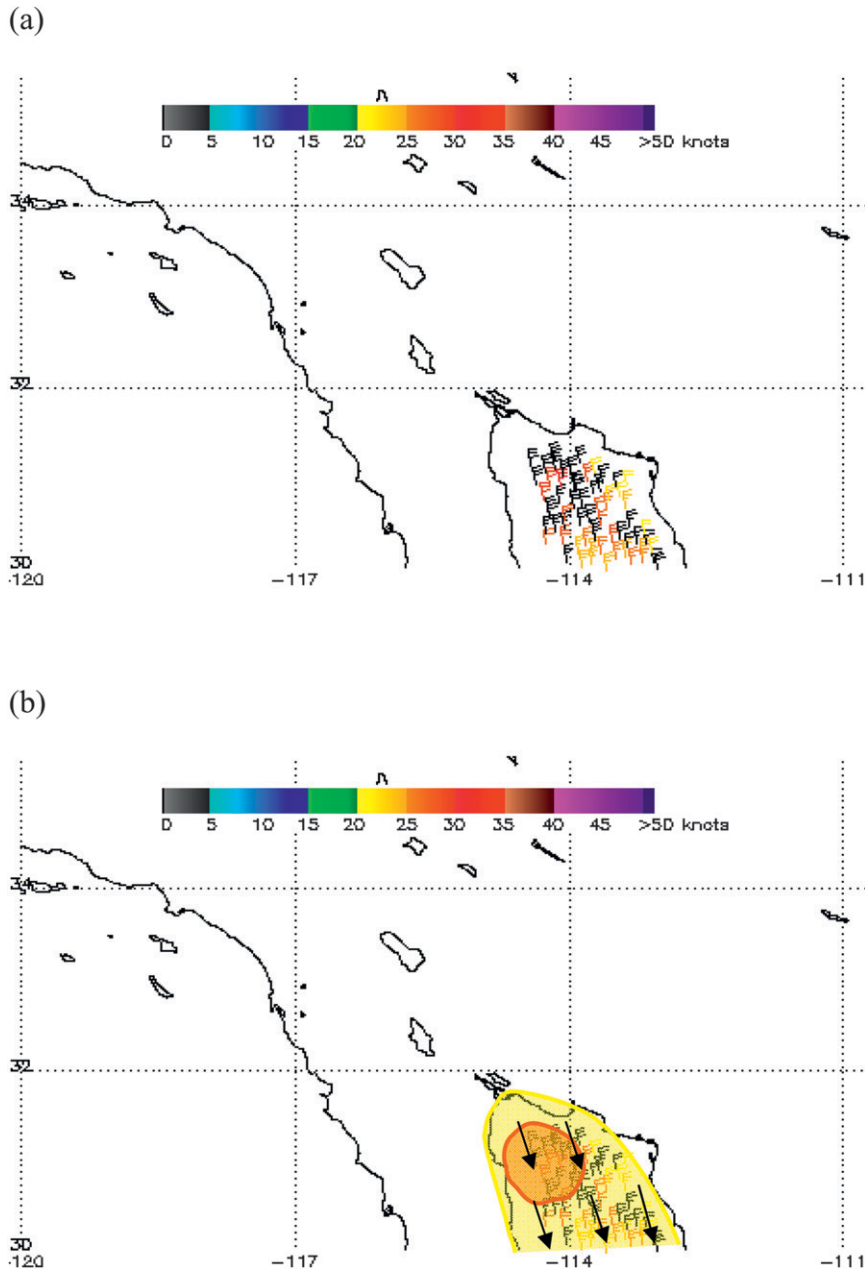


FIG. 17. (a) Corresponding QuikSCAT data around 1250 UTC 14 Oct 2008, which provide swaths ocean wind vectors from the polar-orbiting QuikSCAT satellite. (b) Same as in (a) but with approximate isotachs (yellow indicating 20–29 kt and orange indicating 30+ kt) and arrows plotted in the Gulf of California for comparison with Figs. 16 and 18.

event. In particular, the MM5 appears to accurately predict the rapidity of the initial wind speed increase. Throughout the simulation, the GFS-modeled wind speeds were too weak. Additionally, both the MM5 and GFS accurately handle the timing of wind speed maxima, though neither the GFS nor the MM5 appear to accurately depict the strengths of these peaks. Note that

the MM5-forecasted winds did not reach gale force for the ship's locations. However, gales were still forecast elsewhere for this event from the MM5 output.

The second simulation we will consider was for an event that occurred on 13–14 October 2008. This simulation was initialized at 0000 UTC 11 October 2008. Figure 16 provides 10-m wind speed output from the

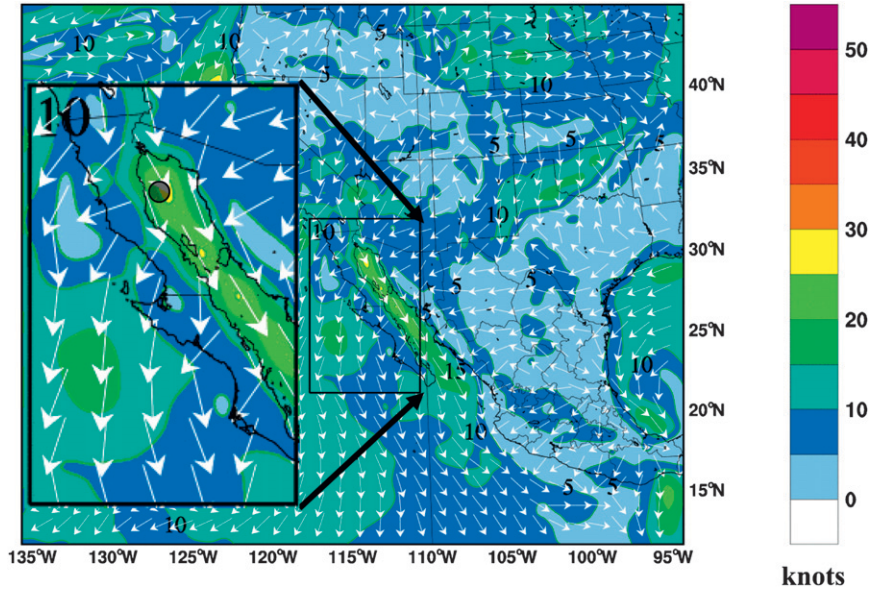


FIG. 18. GFS 10-m wind speed output for a simulation initialized at 0000 UTC 11 Oct 2008 and valid at 1200 UTC 14 Nov 2008 (an 84-h forecast), with the dot indicating the approximate position of the R/V *David Starr Jordan* at this time.

MM5 for 1200 UTC 14 October 2008. Once again, the MM5’s depiction of the near-surface flow across the Gulf of California appears to be more accurate based on the verifying QuikSCAT data from 1250 UTC 14 October 2008 (Fig. 17), especially when compared to that

from the GFS (Fig. 18). The meteogram for this event is plotted in Fig. 19 and also shows better agreement among wind speeds between MM5 output and ship observations for the duration of this event than between GFS output and ship observations. Both the timing of the initial wind

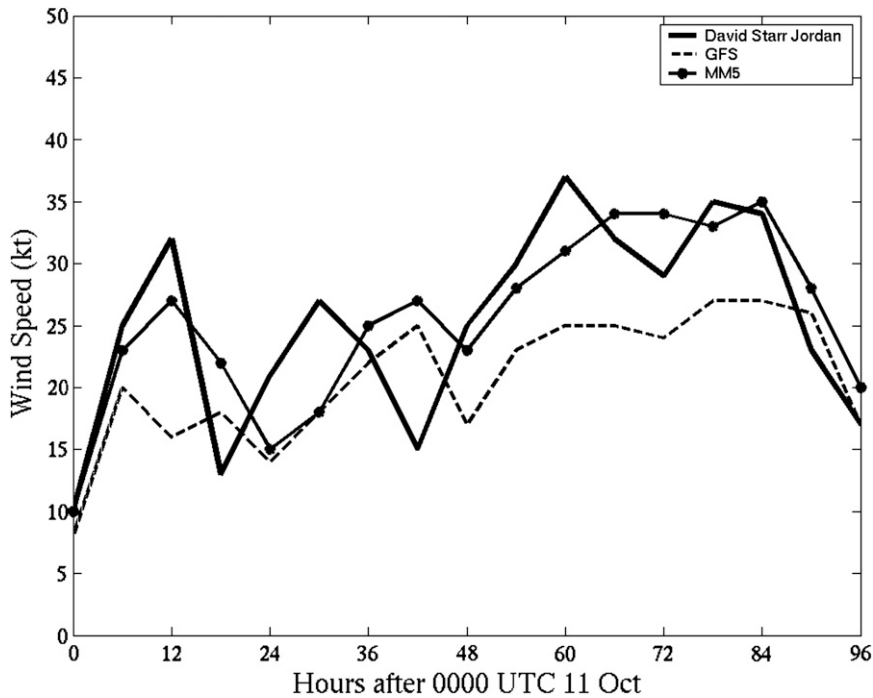


FIG. 19. Meteogram comparing 10-m wind speeds derived from MM5 and GFS for points along the path of the ship, with the corresponding wind speeds measured from the ship.

speed increase and the peaks appear relatively better correlated between the *David Starr Jordan* ship observations and MM5 output than between the observations and the GFS output. Unlike the GFS output, both the MM5 and the observations reach gale force wind speeds during this event.

7. Conclusions

The autumn 2008 mission of the R/V *David Starr Jordan* in the northern Gulf of California detected a number of gale wind events there. The comparison of synoptic distributions during these events to weaker wind events revealed a number of salient synoptic features that drive gale wind events in the Gulf of California. These features consist of a strong surface high pressure system over the northern Rockies, driven by subsidence downstream of a highly amplified long-wave ridge over the east Pacific and western United States, and a low-level front in the northern Gulf of California. The associated steep pressure gradient between the surface high and front was found to funnel a northerly surge of wind into the Gulf of California. Additionally, a shallow unstable layer north of the low-level front provides increased mixing for stronger surface winds beneath a stable layer aloft that traps wave energy. The local terrain also plays a fundamental role in the wind enhancement in the Gulf of California. The MM5 appears to provide an accurate depiction of 10-m wind speeds as compared to QuikSCAT imagery for two of the events considered. Comparisons to the GFS (and several other global models) for this case reveal the need for high-resolution modeling to more accurately depict the strength and geographic structure of these and similar gap wind events.

Acknowledgments. The authors thank the staff of NHC's TAFB for numerous discussions and the motivation to further study gale wind events in the Gulf of California, particularly Mr. Waldemar Barnes and Mr. Eric Christensen. Additionally, this work would not have been made possible without the computing resources provided by Dr. Shuyi Chen and Mr. Derek Ort of the University of Miami's Rosenstiel School of Marine and Atmospheric Sciences and particularly their support in running the MM5 model. We also thank Dr. Chris Landsea and Mr. Todd Kimberlain of the NHC and Mr. Erik Pytlak of the National Weather Service Forecast Office in Tuscon, Arizona, for thorough reviews of earlier editions of this work. Their comments greatly improved the quality of this work, as did the reviews of three anonymous reviewers.

REFERENCES

- Brennan, M. J., C. C. Hennon, and R. D. Knabb, 2009: The operational use of QuikSCAT ocean surface vector winds at the National Hurricane Center. *Wea. Forecasting*, **24**, 621–645.
- Chelton, D. B., and Coauthors, 2001: Observations of coupling between surface wind stress and sea surface temperature in the eastern tropical Pacific. *J. Climate*, **14**, 1479–1498.
- , M. H. Freilich, J. M. Sienkiewicz, and J. M. Von Ahn, 2006: On the use of QuikSCAT scatterometer measurements of surface winds for marine weather prediction. *Mon. Wea. Rev.*, **134**, 2055–2071.
- Cobb, H. D., III, D. P. Brown, and R. Molleda, 2002: Use of QuikSCAT imagery in the diagnosis and detection of Gulf of Tehuantepec wind events 1999–2002. Preprints, *12th Conf. on Satellite Meteorology and Oceanography*, Long Beach, CA, Amer. Meteor. Soc., JP4.1. [Available online at <http://ams.confex.com/ams/pdfpapers/54957.pdf>.]
- Grell, G. A., J. Dudhia, and D. R. Stauffer, 1994: A description of the fifth-generation Penn State/NCAR mesoscale model (MM5). NCAR Tech. Note NCAR/TN-398+STR, 122 pp.
- Kalnay, E., M. Kanamitsu, and W. E. Baker, 1990: Global numerical weather prediction at the National Meteorological Center. *Bull. Amer. Meteor. Soc.*, **71**, 1410–1428.
- , and Coauthors, 1996: The NCEP/NCAR 40-Year Reanalysis Project. *Bull. Amer. Meteor. Soc.*, **77**, 437–471.
- Leslie, L. M., B. W. Buckley, and M. Leplastrier, 2008: The operational impact of QuikSCAT winds in Perth, Australia: Examples and limitations. *Wea. Forecasting*, **23**, 183–193.
- Mass, C. F., and M. D. Albright, 1985: A severe windstorm in the lee of the Cascade Mountains of Washington state. *Mon. Wea. Rev.*, **113**, 1261–1281.
- National Geophysical Data Center, cited 2009: Topographic data and images. [Available online at <http://www.ngdc.noaa.gov/mgg/topo/>.]
- National Weather Service, 2008: Offshore, Navtex, high seas, and marine forecast services. NWSPD 10-3, NWS Instruction 10-311, 46 pp. [Available online at <http://www.nws.noaa.gov/directives/sym/pd01003011curr.pdf>.]
- Reynolds, R. W., and T. M. Smith, 1994: Improved global sea surface temperature analyses using optimum interpolation. *J. Climate*, **7**, 929–948.
- Risien, C. M., and D. B. Chelton, 2008: A global climatology of surface wind and wind stress fields from eight years of QuikSCAT scatterometer data. *J. Phys. Oceanogr.*, **38**, 2379–2413.
- Schultz, D. M., W. E. Bracken, L. F. Bosart, G. J. Hakim, M. A. Bedrick, M. J. Dickinson, and K. R. Tyle, 1997: The 1993 Superstorm cold surge: Frontal structure, gap flow, and tropical impact. *Mon. Wea. Rev.*, **125**, 5–39.
- Sharp, J., and C. F. Mass, 2002: Columbia Gorge gap flow—Insights from observational analysis and ultra-high-resolution simulation. *Bull. Amer. Meteor. Soc.*, **83**, 1757–1762.
- University of Wyoming, cited 2008: Atmospheric soundings. Dept. of Atmospheric Science, University of Wyoming. [Available online at <http://weather.uwyo.edu/upperair/sounding.html>.]
- Von Ahn, J. M., J. M. Sienkiewicz, and P. S. Chang, 2006: The operational impact of QuikSCAT winds at the NOAA Ocean Prediction Center. *Wea. Forecasting*, **21**, 523–539.
- Wallace, J. M., T. P. Mitchell, and C. Deser, 1989: The influence of sea surface temperature on surface wind in the eastern equatorial Pacific: Seasonal and interannual variability. *J. Climate*, **2**, 1492–1499.
- Williams, J., 1996: *The Sea of Cortez*. 3rd ed. Vol. II, *Baja Boater's Guide*, H. J. Williams Publications, 256 pp.